Chemical Science

ROYAL SOCIETY OF CHEMISTRY

EDGE ARTICLE

View Article Online
View Journal | View Issue

Cite this: *Chem. Sci.*, 2021, **12**, 6333

All publication charges for this article have been paid for by the Royal Society of Chemistry

Donor–acceptor–acceptor-type near-infrared fluorophores that contain dithienophosphole oxide and boryl groups: effect of the boryl group on the nonradiative decay†

Yoshiaki Sugihara,‡[a] Naoto Inai,‡[a] Masayasu Taki,[b] Thomas Baumgartner,[c] Ryosuke Kawakami,[d] Takashi Saitou,[d] Takeshi Imamura,[d] Takeshi Yanai *[ab] and Shigehiro Yamaguchi *[ab]

The use of donor–π–acceptor (D–π–A) skeletons is an effective strategy for the design of fluorophores with red-shifted emission. In particular, the use of amino and boryl moieties as the electron-donating and -accepting groups, respectively, can produce dyes that exhibit high fluorescence and solvatochromism. Herein, we introduce a dithienophosphole *P*-oxide scaffold as an acceptor–spacer to produce a boryl- and amino-substituted donor–acceptor–acceptor (D–A–A) π-system. The thus obtained fluorophores exhibit emission in the near-infrared (NIR) region, while maintaining high fluorescence quantum yields even in polar solvents (*e.g.* λ_{em} = 704 nm and Φ_F = 0.69 in CH_3CN). A comparison of these compounds with their formyl- or cyano-substituted counterparts demonstrated the importance of the boryl group for generating intense emission. The differences among these electron-accepting substituents were examined in detail using theoretical calculations, which revealed the crucial role of the boryl group in lowering the nonradiative decay rate constant by decreasing the non-adiabatic coupling in the internal conversion process. The D–A–A framework was further fine-tuned to improve the photostability. One of these D–A–A dyes was successfully used in bioimaging to visualize the blood vessels of Japanese medaka larvae and mouse brain.

Received 10th February 2021
Accepted 24th March 2021

DOI: 10.1039/d1sc00827g

rsc.li/chemical-science

Introduction

Organic π-conjugated compounds with a donor–π–acceptor (D–π–A) framework have attracted substantial attention due to their wide range of applications.[1–8] The absorption and emission properties of D–π–A compounds can be tuned by structural modifications of the individual components. By using an appropriate combination of donor, π-spacer, and acceptor moieties, even near-infrared (NIR) emission can be attained. Such NIR-emissive compounds are promising materials for NIR-emissive OLEDs,[9,10] biosensing applications,[11] and deep-tissue bioimaging given the high biopermeability of the NIR light.[12,13]

Even though various D–π–A-type fluorophores that exhibit NIR emission have been developed so far, their fluorescence quantum yields (Φ_F) tend to decrease drastically in polar solvents. However, D–π–A compounds that contain a diarylboryl moiety as the electron-accepting group represent one exception to this trend.[5–8] In 1972, Williams and co-workers reported a simple *p*-(dimesitylboryl)-substituted triphenylamine as the first example of a boron-based D–π–A-type fluorophore.[14] Since then, boryl-substituted D–π–A dyes have been extensively studied in order to explore their potential utility as nonlinear optical materials,[15,16] two-photon-emissive materials,[17] anion sensors,[18] and bioimaging.[19] These compounds often exhibit high Φ_F values even in polar media, despite the significant red-shift of their emission bands.[5c] Two moieties in this type of molecular frameworks can be modified to obtain NIR emission: the aryl group on the boron atom and the π-spacer. For example, in 2015, Marder and co-workers reported D–π–A compounds with an electron-withdrawing perfluorophenyl or 3,5-$(CF_3)_2C_6H_3$ group at the *para* position of the

[a]*Department of Chemistry, Graduate School of Science, Integrated Research Consortium on Chemical Sciences (IRCCS), Nagoya University, Furo, Chikusa, Nagoya, 464-8602, Japan. E-mail: yanait@chem.nagoya-u.ac.jp; yamaguchi@chem.nagoya-u.ac.jp*

[b]*Institute of Transformative Bio-Molecules (WPI-ITbM), Nagoya University, Furo, Chikusa, Nagoya, 464-8602, Japan*

[c]*Department of Chemistry, York University, 4700 Keele St., Toronto, ON M3J 1P3, Canada*

[d]*Department of Molecular Medicine for Pathogenesis, Graduate School of Medicine, Ehime University, Shitsukawa, Toon City, Ehime, 791-0295, Japan*

† Electronic supplementary information (ESI) available: Experimental details, photophysical properties, evaluation of the photostability, theoretical calculations, *in vivo* imaging, and NMR spectra for all new compounds. See DOI: 10.1039/d1sc00827g

‡ These authors contributed equally to this work.

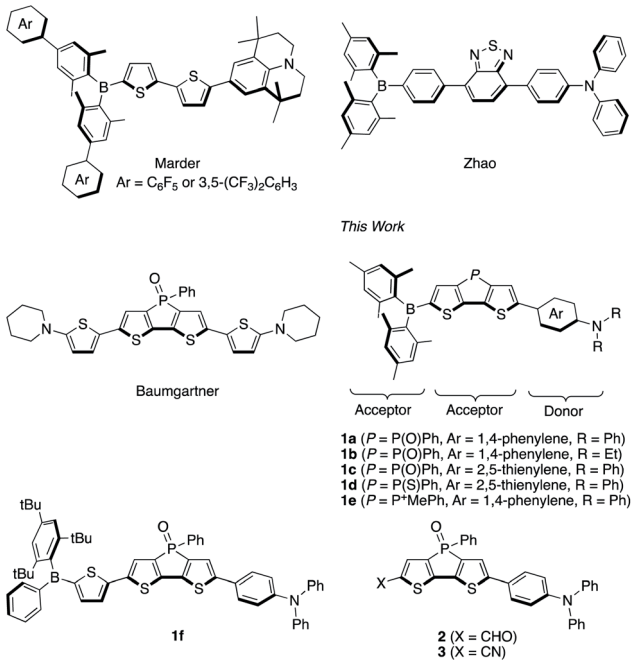

Fig. 1 Representative boryl-substituted D–π–A dyes and dithienophosphole *P*-oxide derivatives and boryl-substituted D–A–A type dyes and relevant compounds studied in this work.

aryl group on the boron atom (Fig. 1).[20] In combination with the strong donor julolidine, the compounds showed NIR fluorescence in CH_3CN with maximum emission wavelengths (λ_{em}) around 745 nm. On the other hand, in 2014, Zhao and co-workers reported a fluorophore that employed 2,1,3-benzothiadiazole as additional electron-accepting π-spacer, emitting in the far-red to NIR region ($\lambda_{em} = 669$ nm) in CH_3CN (Fig. 1).[21] Misra and co-workers achieved a further red-shifted emission ($\lambda_{em} = 692$ nm; $\Phi_F = 0.27$ in CH_2Cl_2) by insertion of acetylene spacers.[22] Such donor–acceptor–acceptor (D–A–A)-type structures should thus be beneficial for achieving red-shifted emission.

To develop NIR-fluorescent dyes, we have focused our attention on the modification of the π-spacer by introducing a phosphine oxide group. We envisioned that the P(=O)Ph group could bathochromically shift the emission by lowering the LUMO energy level due to the σ*–π* interaction[23,24] as well as the inherent inductive electron-withdrawing effect. The profound effect of introducing a phosphine oxide group has already been documented for several fluorescent dyes. For example, fluorescein, a xanthene dye, exhibits a fluorescence maximum at 510 nm, while phospha-fluorescein, a phosphine-oxide-containing fluorescein analogue, exhibits an emission maximum of 656 nm.[25] This example aptly illustrates the substantial impact of the phosphine oxide group on the electronic structure.

In this context, dithieno[3,2-*b*:2′,3′-*d*]phosphole *P*-oxide represents an attractive scaffold. Various dithienophosphole derivatives have already been developed by expanding its π-skeleton or modifying the *P*-aryl groups.[26,27] While dithienophosphole *P*-oxide itself exhibits an emission maximum at 453 nm in CH_2Cl_2, its emission wavelength can be red-shifted by introducing electron-donating triphenylamine moieties at its termini.[28] The incorporation of the stronger donor moiety aminothiophene further red-shifts the emission to 657 nm with a moderate fluorescence quantum yield ($\Phi_F = 0.39$) in CH_2Cl_2 (Fig. 1).[29]

In this article, we report the design and synthesis of boryl-substituted D–A–A-type fluorophores, which contain a dithienophosphole *P*-oxide scaffold as an additional acceptor moiety, as highly emissive NIR-fluorescent dyes (Fig. 1). The phosphine oxide group was expected to red-shift the emission band, improve the photostability of the dye, and afford a more rigid molecular structure, which would suppress the nonradiative decay process and thus improve the quantum yield. A series of the D–A–A type dyes **1a–1f** that bear various aryl groups on the boron atom, phosphorus-substitution patterns, and electron-donating moieties was synthesized, and their substituent effects were studied in-depth in order to accomplish intense NIR emission and high photostability. A comparative study with other D–A–A type analogues **2** and **3** with different acceptor units in place of the boryl group (Fig. 1) revealed the important role of a terminal boryl group to suppress the non-radiative decay process, resulting in the high fluorescence quantum yields, according to excited-state theoretical calculations. To demonstrate the utility of such dyes, **1c** was employed for fluorescence imaging *in vivo*.

Results and discussion

Compounds **1a–1f** were synthesized using 2,6-dibromodithienophosphole *P*-oxide **4**[28a] as the key precursor (Scheme 1). The crucial step in the synthesis of **1a–1e** is the mono-functionalization of **4**. Its reduction with trichlorosilane, followed by treatment with 1.1 equiv. of *n*-BuLi produced mainly the mono-lithiated product, which was successively treated with Mes_2BF. Further oxidation with pyridinium chlorochromate (PCC) or sulfur afforded **5** or **6** in 24% and 18% overall yield, respectively. Suzuki–Miyaura cross-coupling of **5** or **6** with the corresponding amino-substituted arylboronic acid or boronic ester afforded **1a–1d** in moderate yields. The phosphonium derivative **1e** was obtained by the reduction of **1a**, followed by methylation of the P centre with MeOTf. Subsequent recrystallization from a hexane/$CHCl_3$ mixed solvent afforded **1e**.

For the synthesis of **1f**, bearing a bulky tri(*t*-butyl)phenyl group on the boron atom, mono-arylation of the key precursor **4** was employed. Specifically, the Suzuki–Miyaura cross-coupling of **4** with 1.0 equiv. of diphenylaminophenylboronic acid furnished **7**, which was subsequently coupled with borylthienylboronic ester **8**, obtained *in situ* from the direct borylation of the corresponding thienylborane precursor using an Ir catalyst, to generate **1f** (for details, see the ESI†). Compounds **1a–1f** are sufficiently stable to be handled in air without any special precautions.

The formyl- and cyano-substituted analogues **2** and **3** were synthesized as reference compounds (*vide infra*) *via* the mono-lithiation of **4**; *i.e.*, following the reduction of **4** and its

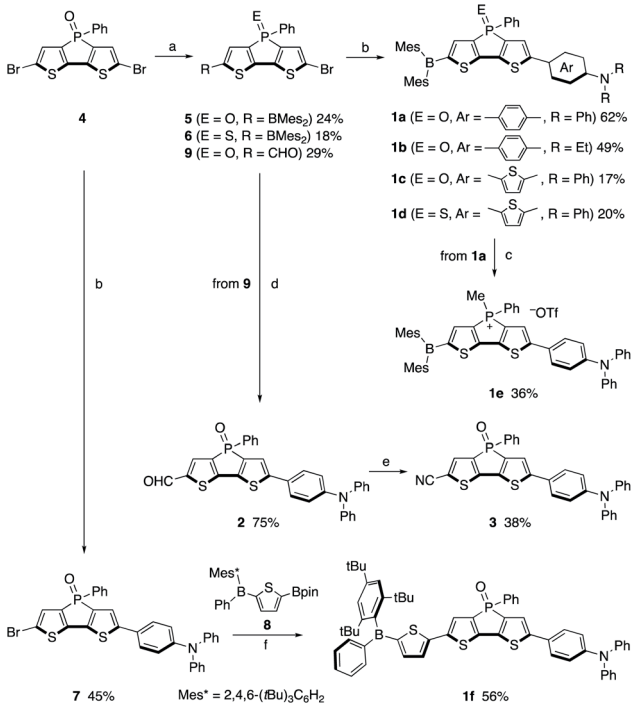

Scheme 1 Synthesis of compounds **1a–1f**, **2**, and **3**. Reagents and conditions: (a) (1) $HSiCl_3$, toluene, rt; (2) *n*-BuLi, THF, −78 °C; (3) Mes_2BF or DMF, THF, −78 °C to rt; (4) PCC, S_8, or H_2O_2, CH_2Cl_2, rt; (b) 4-$(Ph_2N)C_6H_4B(OH)_2$, 4-$(Et_2N)C_6H_4B(OH)_2$, or 2-(Ph_2N)-5-(pin)B-thiophene, $Pd(PPh_3)_4$, K_2CO_3, toluene, 110 °C; (c) (1) $HSiCl_3$, toluene, rt; (2) MeOTf, CH_2Cl_2, rt; (d) (1) ethylene glycol, TsOH·H_2O, benzene, 100 °C, (2) 4-$(Ph_2N)C_6H_4B(OH)_2$, $Pd(PPh_3)_4$, Na_2CO_3, toluene/H_2O, (3) HCl_{aq}; (e) $H_2NOH{\cdot}HCl$, TsOH·H_2O, $MgSO_4$, toluene, 120 °C; (f) $Pd(PPh_3)_4$, Na_2CO_3, toluene/H_2O, 110 °C.

lithiation with 1.1 equiv. of *n*-BuLi, DMF was added as the formyl source. Further oxidation of the phosphine moiety with H_2O_2 afforded **9**. After protection of the formyl group, Suzuki–Miyaura cross-coupling and subsequent deprotection of the acetal moiety afforded **2**. Transformation of the formyl group in **2** into a cyano group using hydroxylamine afforded **3**.

Photophysical properties of D–A–A dye 1a

Initially, we evaluated the photophysical properties of **1a**, summarized in Table 1, and the UV-vis absorption and fluorescence spectra of **1a** in various solvents are shown in Fig. 2a. Regardless of the solvent used, **1a** showed absorption maxima (λ_{abs}) at 458–466 nm with molar absorption coefficients >30 000 M^{-1} cm^{-1}. In contrast, the fluorescence spectra of **1a** exhibited significant solvatochromism. While **1a** showed an emission maximum (λ_{em}) at 532 nm with a Stokes shift of 3037 cm^{-1} in nonpolar cyclohexane, a significant bathochromic shift (λ_{em} = 665 nm) with a large Stokes shift (6607 cm^{-1}) was observed in polar CH_3CN. This result demonstrates that **1a** exhibits a strong intramolecular charge-transfer (ICT) character in the excited state, which is a typical feature of D–π–A fluorophores. The ICT character of **1a** is also reflected in a large dipole moment in the excited state (μ_E = 20.6 D), which was estimated using the Lippert–Mataga equation (Fig. S8 and Table S2†). Notably, **1a** maintained a high fluorescence quantum yield in polar solvents (*e.g.*, in CH_3CN: $\Phi_F = 0.59$) despite its large μ_E value. This behaviour differs significantly from that commonly seen in D–π–A-type fluorescent dyes.

Effects of the boryl group on the photophysical properties

To investigate the origin of the high fluorescence quantum yield of **1a**, especially in polar solvents, its photophysical properties

Table 1 Photophysical properties of D–A–A-type dyes **1a–1f** and reference compounds **2** and **3** in various solvents

Compound	Solvent	λ_{abs}[a] (nm)	ε (10^4 M^{-1} cm^{-1})	λ_{em} (nm)	Stokes shift (cm^{-1})	Φ_F[b]	k_r (10^8 s^{-1})	k_{nr} (10^8 s^{-1})
1a	Cyclohexane	458	3.56	532	3037	0.81	2.6	0.62
	Toluene	466	3.43	566	3791	0.90	2.8	0.31
	$CHCl_3$	466	3.18	597	4709	0.90	2.3	0.25
	CH_2Cl_2	466	3.32	626	5485	0.88	2.1	0.28
	CH_3CN	462	3.45	665	6607	0.59	1.5	1.0
1b	Cyclohexane	470	3.26	540	2758	0.81	2.3	0.54
	CH_3CN	487	3.28	695	6145	0.72	1.5	0.59
1c	Cyclohexane	486	3.14	570	3032	0.65	1.9	0.99
	CH_3CN	477	2.77	704	6760	0.67	1.5	0.74
1d	Cyclohexane	476	3.07	567	3372	0.86	2.4	0.39
	CH_3CN	475	2.77	699	6848	0.69	1.5	0.67
1e	Cyclohexane	488	—[c]	617	4284	0.62	n.d.	n.d.
	CH_3CN	480	2.67	748	7464	0.07	n.d.	n.d.
1f	Cyclohexane	470	4.47	550	3095	0.44	2.0	2.6
	CH_3CN	474	4.70	651	5736	0.71	1.8	0.72
2	Cyclohexane	463	2.44	537	2976	0.60	1.5	1.0
	CH_3CN	464	2.70	709	7447	0.08	0.94	11
3	Cyclohexane	453	—[c]	548	3827	0.59	1.4	0.98
	CH_3CN	452	2.46	681	7440	0.26	0.95	2.7

[a] Only the longest absorption maximum wavelengths are shown. [b] Absolute fluorescence quantum yields were determined by a calibrated integrating sphere system within ±3% error. [c] Not determined due to poor solubility.

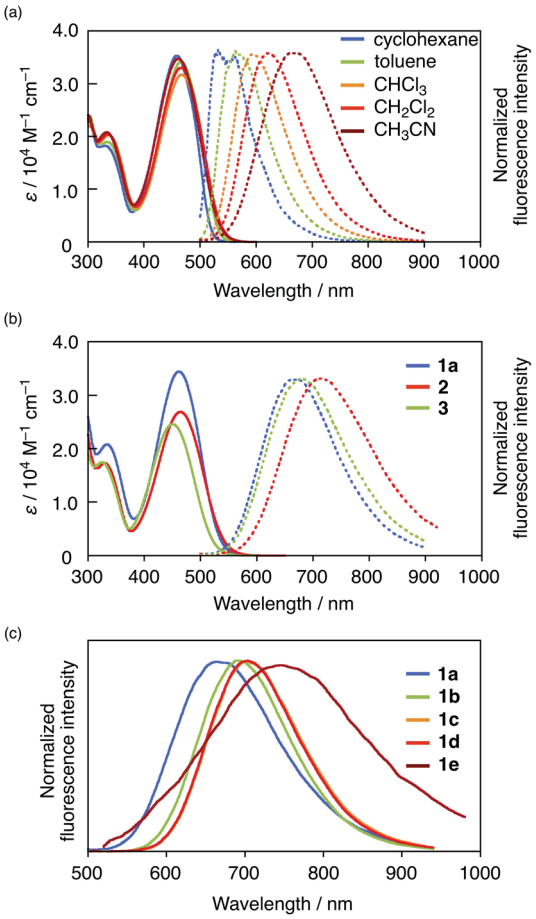

Fig. 2 UV-vis absorption and emission spectra of (a) **1a** in various solvents, (b) **1a**, **2**, and **3** in CH_3CN, and (c) emission spectra of **1a**–**1e** in CH_3CN.

were compared to those of reference compounds **2** and **3**, which contain a formyl and cyano group instead of the boryl group, respectively. While cyano analogue **3** showed a maximum emission wavelength slightly longer than that of **1a** in CH_3CN, formyl analogue **2** exhibited a more red-shifted emission ($\Delta\lambda$ = 44 nm; Fig. 2b). Moreover, **2** and **3** also showed significant solvent effects, *i.e.*, large dipole moments (**2**: μ_E = 23.8 D; **3**: μ_E = 21.0 D) were estimated using the Lippert–Mataga equation (Fig. S8†), which suggests strong ICT character in the excited state, akin to that of **1a**. However, their fluorescence quantum yields decreased drastically in polar solvents such as CH_3CN (**2**: Φ_F = 0.08; **3**: Φ_F = 0.26), which is typical for D–π–A-type dyes.

To gain further insight into the features of boryl-substituted fluorescent dye **1a**, we examined its excited-state dynamics in terms of its radiative (k_r) and nonradiative (k_{nr}) decay rate constants from the excited singlet state (S_1). These values are determined by the Φ_F values and the fluorescence lifetimes τ. For **1a**, **2**, and **3**, the k_r values decrease with increasing solvent polarity (Table 1). Boryl derivative **1a** exhibits a higher k_r value than **2** or **3** in CH_3CN, which is at least partially responsible for its higher Φ_F value. Moreover, **1a** shows the lowest k_{nr} value in $CHCl_3$, which increases slightly in CH_3CN. Importantly, the k_{nr} value of **1a** in CH_3CN is 1.0×10^8 s^{-1}, while those of **2** and **3** are beyond 10^8 s^{-1}. These results indicate that not only the higher k_r value, but also the suppressed k_{nr} value are responsible for the high fluorescence quantum yield of **1a** in polar solvents.

Theoretical examination of the effects of the boryl group

A theoretical analysis of the photophysical properties of the diarylboryl and dithienophosphole-based D–A–A type molecules was carried out using time-dependent density functional theory (TD-DFT). As the characteristic effects of the boryl group in **1a** on Φ_F were experimentally observed in comparison with reference compounds **2** and **3**, this computational study was focused on the elucidation of the role of the boryl group in increasing Φ_F. The solvent effects were considered using the polarizable continuum model (PCM) to verify their impact on Φ_F. The calculations were designed to identify the major factors that determine k_r and k_{nr} (for the details of the computational calculations, see the ESI†).

First, the radiative transition relevant to the k_r value was examined based on the TD-DFT results in S_0 and S_1 (Fig. 3). Boryl derivative **1a** exhibits a slightly higher oscillator strength (f = 1.19) for the Franck–Condon transition from S_0 to S_1 relative to **2** (f = 1.02) and **3** (f = 0.97). This result is consistent with the fact that **1a** exhibits a ~50% higher molar absorption coefficient than **2** and **3**. Notably, the f value for the vertical transition from S_1 to S_0 for **1a** with the optimized S_1 geometry is also higher than those for **2** and **3** (**1a**: f = 1.42; **2**: 1.34; **3**: 1.26, Fig. S13†). As k_r is proportional to $\nu^2 f$, where ν is the wavenumber of the emission, the higher f value in **1a** should be partially responsible for the higher k_r value relative to those of **2** and **3**.

Next, we examined the non-radiative transition relevant to the k_{nr} value, which may occur through various decay processes. The possible pathways include the internal

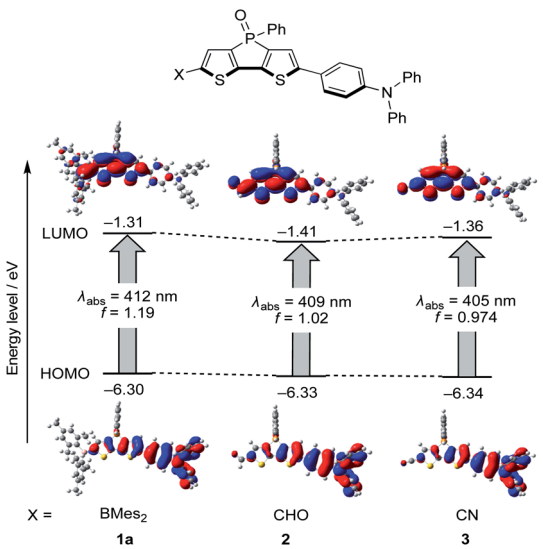

Fig. 3 Energy diagrams for the frontier orbitals of **1a**, **2**, and **3** in CH_3CN using the optimized ground state structures. Calculations were carried out at the CAM-B3LYP/6-31G(d) level of theory including the PCM model.

conversion (IC) from S_1 to S_0 and/or the intersystem crossing (ISC) to the triplet states.[30] We performed rate-constant calculations on the $S_1 \rightarrow S_0$ IC process and the $S_1 \rightarrow T_2$ ISC process; hereafter, their rates are denoted as k_{IC} and k_{ISC}, respectively. With the relaxed S_1 geometry, S_1 and T_2 lie closely in energy and largely away from other states, which were thus neglected (Fig. S14†). The k_{IC} and k_{ISC} of **1a** in CH_3CN were estimated to be 1.4×10^8 and 1.0×10^7 [s^{-1}], respectively, using MOMAP-2020A program[31] (for details, see the ESI†). This implies that the main nonradiative decay pathway of these dyes in CH_3CN is the $S_1 \rightarrow S_0$ IC.

To discuss the relative trend of the experimentally obtained k_{nr} values among **1a**, **2**, and **3**, which are assumed to be mainly k_{IC}, the normal-mode contribution of the nonadiabatic coupling (NAC) calculated with the S_1-optimized geometry was analysed as shown in Fig. 4a. For all compounds, the normal mode with a frequency of *ca.* 1570 cm^{-1} was found to have one of the largest NAC values (Fig. S15†). These modes were attributed mainly to the C5–C6 and C7–C8 stretching vibration in the bithiophene moiety of the dithienophosphole scaffold (for the atom labelling, see Fig. 4b). Because the largest geometry changes occur in the C5–C6 bond length between the optimized structures of S_0 and S_1, while they are nearly identical among **1a**, **2**, and **3** (Fig. S16†), this quinoidal mode should thus make the largest contribution to k_{IC} through large nonadiabatic interstate coupling.[32]

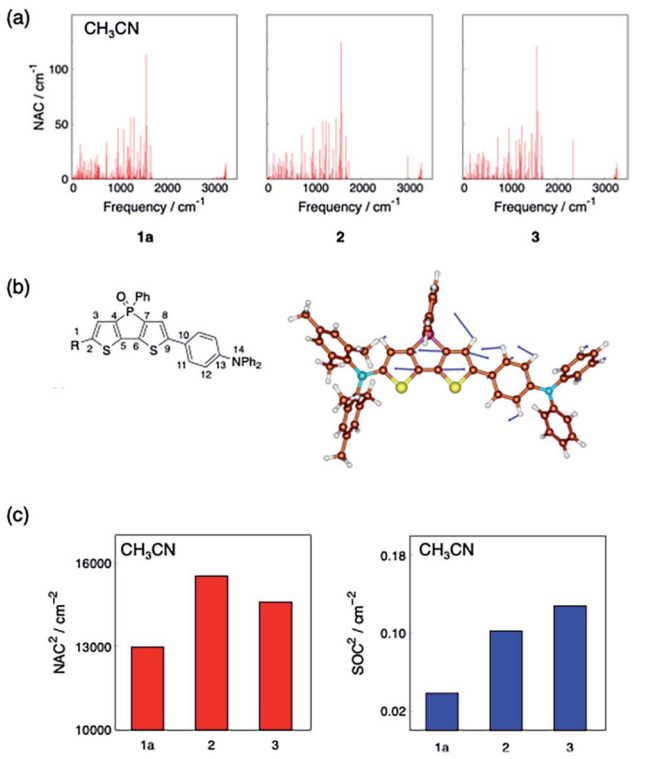

Fig. 4 (a) Computed NAC and frequencies along with the normal modes of **1a**, **2** and **3** in CH_3CN. (b) A representative vibrational mode with large NAC of **1a** in CH_3CN, which has a large contribution of the C5–C6 and C7–C8 stretching and a frequency of 1572 cm^{-1}; the representative vibrational modes of the other molecules are shown in Fig. S15.† (c) Comparison of the square of the largest NAC in Fig. 4a (left) and the square of the SOC between S_1 and T_2 (right) among **1a**, **2** and **3** in CH_3CN. Quantum mechanical calculations were conducted at the (TD-)CAM-B3LYP/6-31G(d) level of theory using Gaussian 16 Rev. B.01 program.[33] SOC were computed using PySOC program.[34]

The NAC values along with the quinoidal mode were calculated to be 113.9 cm^{-1}, 124.6 cm^{-1} and 120.8 cm^{-1} in CH_3CN for **1a**, **2**, and **3**, respectively. Assuming that this mode is the promoting mode of the $S_1 \rightarrow S_0$ IC and vibrational terms are comparable among these dye molecules, the k_{IC} should be proportional to the square of NAC along with this mode. The square of these NAC values provides the following relation: **1a** < **3** < **2** (Fig. 4c). This trend qualitatively matches the relative magnitude of the experimental k_{nr} among the three compounds in CH_3CN. For the CH_3CN solutions, we can thus deduce that the substituent-dependence of k_{IC}, which almost coincides with k_{nr}, is determined by the NACs associated with the quinoidal vibration.

The spin–orbit coupling (SOC) between S_1 and T_2 was also computed. In the procedure here, SOC was treated as a constant. This means that k_{ISC} is proportional to the square of SOC when vibrational terms are comparable among these dye molecules. Compound **1a** has a smaller square of the SOC than the other molecules (Fig. 4c), which implies that **1a** has smaller k_{ISC} than the others.

Considering that the experimentally obtained k_{nr} for **2** was about 10 times larger than that for **1a**, our prediction might underestimate the interstate interaction of **2**. This seemingly arises from the limitation of our model, where the terms that can be important in the calculation of k_{ISC} with small direct SOC (see the ESI† for details) were neglected.

Thus, the question of why boryl derivative **1a** exhibits a larger Φ_F ($= k_r/(k_r + k_{nr})$) compared to **2** and **3** can be partially addressed by our theoretical model, which shows that **1a** in S_1 undergoes decay processes with a larger radiative decay rate constant k_r and a smaller non-radiative decay rate constant k_{nr}. The latter can be rationalized in terms of a suppression of the nonadiabatic IC process with the smaller NACs and the ISC process with smaller SOC.

Structural modification to achieve NIR emission

To accomplish a more red-shifted emission, we modified the donor moiety, π-spacer, and/or the phosphorus moiety of the D–A–A framework (Fig. 2c). The photophysical properties of the corresponding compounds **1b–1e** are summarized in Table 1 (for the full data in various solvents, see Table S1†). Compound **1b**, which contains ethyl groups in place of phenyl groups on the amino moiety, and **1c**, which contains a thiophene π-spacer, exhibited more red-shifted emission bands than **1a** in CH_3CN due to their enhanced electron-donating character (**1b**: λ_{em} = 695 nm; **1c**: λ_{em} = 699 nm). Compound **1d**, in which the P=O bond of **1c** is replaced with a P=S bond, exhibited a comparable emission to that of **1c**. Although **1e**, with a quaternized P centre, showed the longest wavelength emission (λ_{em} = 748 nm in CH_3CN), its Φ_F value was low (0.07). Notably, all these derivatives, except for **1e**, retained high quantum yields even in CH_3CN, despite their long-wavelength emission.

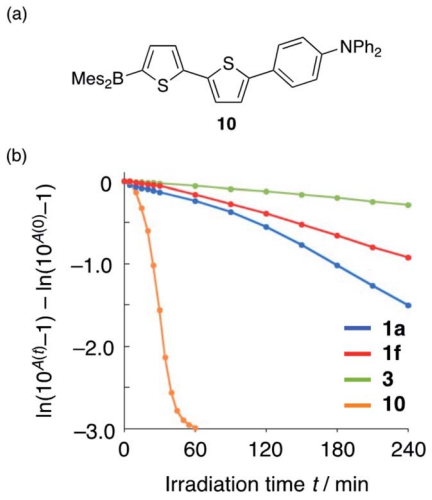

Fig. 5 (a) Chemical structure of **10** and (b) monitoring the absorption decay upon exposure to irradiation from LED light (λ_{em} = 449 nm).

Evaluation of the photostability

The introduction of additional heteroatoms can be expected to affect the photostability of the present compounds.[35] Therefore, the photostability of **1a**, **3**, and reference compound **10** (Fig. 5a), which does not contain a P(=O)Ph group, was evaluated in degassed CH_3CN under irradiation from a 449 nm high-power LED lamp equipped with a 450/10 nm hard-coated bandpass filter. We have previously demonstrated that the introduction of a bulky substituent on the B atom results in increased photostability.[36] Accordingly, we designed **1f**, which should exhibit improved photostability relative to **1a**, on account of the bulky substituent at the boron atom, and evaluated its photophysical properties. To quantitatively evaluate the photostability of these compounds, we attempted to determine their total quantum yield of photodecomposition (Φ_{dec}), which is defined as the sum of the quantum yields of all photoreactions producing products under light irradiation.[37–39] The Φ_{dec} values estimated were considered to be the minimum possible values, as Φ_{dec} is underestimated when the decomposition products absorb light at the monitored wavelength.

The results of the irradiation experiments are shown in Fig. 5b. While the change in absorbance over time was almost linear for **3** and **1f**, **1a** and **10** showed non-linear behaviour, probably due to the influence of the absorption of the photodecomposed product(s). Although the Φ_{dec} values for **1a** and **10** cannot be determined quantitatively, given that a linear slope value is required for the calculation, a qualitative comparison demonstrates that **1a** is substantially more photostable than **10**, confirming that the introduction of the P(=O)Ph group improves the photostability of the fluorophore. Furthermore, bulky aryl-substituted **1f** showed improved photostability ($\Phi_{dec} = 5.8 \times 10^{-6}$). This value approaches that of **3** (2.7×10^{-6}) and is two orders of magnitude smaller than that of Alexa Fluor 488 (2.3×10^{-4} in DMSO/buffer = 7/3), which is widely used as a representative photostable dye in bioimaging. However, it should be noted here that these values cannot be compared directly as different solvents were used in the measurements. The improved photostability of **1f** suggests that the steric congestion around the boron atom greatly enhances its photostability.

Application to bioimaging

The bright far-red to NIR emission of the D–A–A dyes **1**, even in polar solvents, suggest promising potential for fluorescence imaging of biological samples. To examine the utility of these dyes in such applications, **1c** was employed as a representative example. Prior to conducting the imaging experiments, we confirmed the solubility of **1c** in phosphate-buffered saline (PBS; pH = 7.4) containing 2% bovine serum albumin (BSA), which is the most abundant protein in the blood plasma, by dynamic light scattering (DLS) measurements (Fig. S17†). The solution of **1c** in the presence of BSA only showed a peak comparable to that of a solution of BSA without **1c**, indicating that **1c** was solved under these conditions. Moreover, the solution exhibited red fluorescence with a λ_{em} of 632 nm (Fig. S18†), which is slightly shorter than that in $CHCl_3$. This fact implies that **1c** is bound to the hydrophobic pocket of BSA.[40]

With these results in hand, we tested **1c** in two kinds of imaging. First, we used **1c** for the *in vivo* imaging of blood vessels in Japanese medaka (*Oryzias latipes*) larvae one week after hatching. For that purpose, a solution of **1c** in DMSO (<1 μL, 1 mM) was directly injected into the peritoneal cavity of the fish using a microinjection system. The fish was then placed into water with 0.3% salinity and cultured for 1 h. We conducted a whole-body imaging analysis of the larvae using a confocal microscopy system (λ_{ex} = 488 nm; emission collection: 570–620 nm). Fig. 6a shows a 3D image of the fish that was reconstructed by combining five 1272.8 μm × 1272.8 μm × 918 μm images; as shown, the blood vessels are clearly visible in the living fish. This result suggests that **1c** is rapidly absorbed into the bloodstream, where it most likely binds to proteins such as albumin.

Then, we performed deep imaging of the blood vessels in mouse brain using two-photon excitation microscopy. Immediately after administering 100 μL of **1c** (0.9 mM in PBS containing 18% DMSO and 1.6% BSA) to a mouse *via* intravenous injection, images were recorded through an open-skull window at a two-photon excitation wavelength of 880 nm (Fig. 6b). Notably, in addition to emission of the dye in the bloodstream in the red region (λ_{em} = 601–657 nm), some blood vessels also exhibited green fluorescence in the 500–550 nm region, which indicates that the microenvironment of the dye is considerably

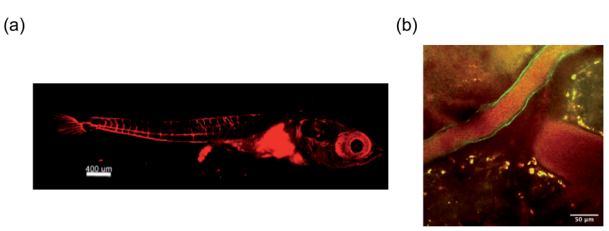

Fig. 6 (a) Confocal image of the entire body of a Japanese medaka larvae and (b) two-photon excitation image of blood vessels in mouse brain.

hydrophobic. Although the identity of the biological component that is stained with **1c** to produce this green fluorescence has not yet been clarified, its observation suggests that the hydrophobic dye may have detached from the albumin and then adsorbed on the hydrophobic region of the blood vessel wall.

Conclusions

We have developed a series of diarylboryl and dithienophosphole *P*-oxide-containing D–A–A-type fluorophores, which exhibit far-red to NIR emissions. Thus, the tuning of the acceptor–spacer is a complementary useful strategy for gaining such red-shifted emissions with the conventional modification of the terminal acceptor boryl group in the D–π–A scaffolds.[20] Unlike analogues that bear formyl or cyano groups in place of the boryl group, the boryl-substituted D–A–A-type fluorophores retain a high fluorescence quantum yield even in polar solvents such as CH_3CN. An analysis of the excited-state dynamics revealed that the higher k_r and the lower k_{nr} values of the developed dyes are responsible for the high quantum yields. TD-DFT calculations demonstrated that the higher k_r values can be attributed to higher oscillator strengths for the electronic transition from S_1 to S_0. In terms of nonradiative decay, the internal conversion from S_1 to S_0 is likely a major pathway, in which the boryl group contributes to decreasing the non-adiabatic coupling associated with the quinoidal stretching mode of the dithienophosphole oxide moiety. This result should provide an important insight into the effect of the boryl groups in the widely studied boron-based D–π–A fluorophores. The introduction of the P(=O)Ph group also greatly influences the photostability of the dyes; the presence of bulky substituents on the boron atom improves the photostability. Moreover, one of the synthesized dyes, **1c**, was successfully applied for whole-body imaging of blood vessels and two-photon bioimaging.

Author contributions

S. Y. and Y. S. conceived the idea. Y. S. synthesized all the compounds and evaluated their properties. N. I. and T. Y. conducted the theoretical calculations. M. T., R. K., T. S., and T. I. conducted imaging experiments. S. Y. and T. B. discussed the π-electron systems studied. Y. S., N. I., M. T., T. Y., and S. Y. wrote the manuscript, and all authors discussed and commented on the manuscript. S. Y. directed the project.

Ethical statement

All animal experiments were approved by the Ethics Committee for Animal Experiments of Ehime University (#05-RE-4-16). The experimental procedures we employed were conducted in accordance with the approved guidelines.

Conflicts of interest

There are no conflicts to declare.

Acknowledgements

This work was supported by MEXT/JSPS KAKENHI Grant Numbers JP18H03909 and JP18H05261 (to S. Y.), JP16H06280 (ABiS), JP15H05952 (to T. I. and T. S.), JP19K12218 and JP20H05038 (to T. S.) and by AMED Grant Number JP20gm1210001 (to T. I.). This work was also funded by Nakatani Foundation for Advancement of Measuring Technologies in Biomedical Engineering, and Kato Memorial Bioscience Foundation (to T. S.). ITbM is supported by the World Premier International Research Center (WPI) Initiative, Japan. T. B. thanks the Canada Research Chairs program for support.

Notes and references

1 (*a*) H. Meier, *Angew. Chem., Int. Ed.*, 2005, **44**, 2482–2506; (*b*) F. Bureš, *RSC Adv.*, 2014, **4**, 58826–58851.
2 (*a*) M. Kivala and F. Diederich, *Acc. Chem. Res.*, 2009, **42**, 235–248; (*b*) S. Kato and F. Diederich, *Chem. Commun.*, 2010, **46**, 1994–2006.
3 (*a*) M. Liang and J. Chen, *Chem. Soc. Rev.*, 2013, **42**, 3453–3488; (*b*) J.-M. Ji, H. Zhou and H. K. Kim, *J. Mater. Chem. A*, 2018, **6**, 14518–14545; (*c*) L. Dou, Y. Liu, Z. Hong, G. Li and Y. Yang, *Chem. Rev.*, 2015, **115**, 12633–12665.
4 J. V. Jun, D. M. Chenoweth and E. J. Petersson, *Org. Biomol. Chem.*, 2020, **18**, 5747–7563.
5 (*a*) C. D. Entwistle and T. B. Marder, *Angew. Chem., Int. Ed.*, 2002, **41**, 2927–2931; (*b*) C. D. Entwistle and T. B. Marder, *Chem. Mater.*, 2004, **16**, 4574–4585; (*c*) L. Ji, S. Griesbeck and T. B. Marder, *Chem. Sci.*, 2017, **8**, 846–863.
6 Z. M. Hudson and S. Wang, *Acc. Chem. Res.*, 2009, **42**, 1584–1596.
7 S. Yamaguchi and A. Wakamiya, *Pure Appl. Chem.*, 2006, **78**, 1413–1424.
8 (*a*) F. Jäkle, *Chem. Rev.*, 2010, **110**(7), 3985–4022; (*b*) Y. Ren and F. Jäkle, *Dalton Trans.*, 2016, **45**, 13996–14007.
9 A. Zampetti, A. Minotto and F. Cacialli, *Adv. Funct. Mater.*, 2019, **29**, 1807623.
10 (*a*) Y. Yuan, Y. Hu, Y.-X. Zhang, J.-D. Lin, Y.-K. Wang, Z.-Q. Jiang, L.-S. Liao and S.-T. Lee, *Adv. Funct. Mater.*, 2017, **27**, 1700986; (*b*) D.-H. Kim, A. D'Aléo, X.-K. Chen, A. D. S. Sandanayaka, D. Yao, L. Zhao, T. Komino, E. Zaborova, G. Canard, Y. Tsuchiya, E. Choi, J. W. Wu, F. Fages, J.-L. Brédas, J.-C. Ribierre and C. Adachi, *Nat. Photonics*, 2018, **12**, 98–104; (*c*) H. Ye, D. H. Kim, X. Chen, A. S. D. Sandanayaka, J. U. Kim, E. Zaborova, G. Canard, Y. Tsuchiya, E. Y. Choi, J. W. Wu, F. Fages, J.-L. Brédas, A. D'Aléo, J.-C. Ribierre and C. Adachi, *Chem. Mater.*, 2018, **30**, 6702–6710; (*d*) D. G. Congrave, B. H. Drummond, P. J. Conaghan, H. Francis, S. T. E. Jones, C. P. Grey, N. C. Greenham, D. Credgington and H. Bronstein, *J. Am. Chem. Soc.*, 2019, **141**, 18390–18394; (*e*) J. Xue, Q. Liang, R. Wang, J. Hou, W. Li, Q. Peng, Z. Shuai and J. Qiao, *Adv. Mater.*, 2019, **31**, 1808242; (*f*) Q. Liang, J. Xu, J. Xue and J. Qiao, *Chem. Commun.*, 2020, **56**, 8988–8991.
11 T. Yamanaka, H. Nakanotani, S. Hara, T. Hirohata and C. Adachi, *Appl. Phys. Express*, 2017, **10**, 074101.

12 S. Zhu, R. Tian, A. L. Antaris, X. Chen and H. Dai, *Adv. Mater.*, 2019, **31**, 1900321.

13 (*a*) Q. Yang, Z. Ma, H. Wang, B. Zhou, S. Zhu, Y. Zhong, J. Wang, H. Wan, A. Antaris, R. Ma, X. Zhang, J. Yang, X. Zhang, H. Sun, W. Liu, Y. Liang and H. Dai, *Adv. Mater.*, 2017, **29**, 1605497; (*b*) Q. Yang, Z. Hu, S. Zhu, R. Ma, H. Ma, Z. Ma, H. Wan, T. Zhu, Z. Jiang, W. Liu, L. Jiao, H. Sun, Y. Liang and H. Dai, *J. Am. Chem. Soc.*, 2018, **140**, 1715–1724.

14 (*a*) J. C. Doty, B. Babb, P. J. Grisdale, M. Glogowski and J. L. R. Williams, *J. Organomet. Chem.*, 1972, **38**, 229–236; (*b*) S. M. Berger, M. Ferger and T. B. Marder, *Chem.–Eur. J.*, 2021, DOI: 10.1002/chem.202005302.

15 (*a*) Z. Yuan, N. J. Taylor, T. B. Marder, I. D. Williams, S. K. Kurtz and L.-T. Cheng, *J. Chem. Soc., Chem. Commun.*, 1990, 1489–1492; (*b*) Z. Yuan, J. C. Collings, N. J. Taylor, T. B. Marder, C. Jardin and J.-F. Halet, *J. Solid State Chem.*, 2000, **154**, 5–12; (*c*) Z. Yuan, C. D. Entwistle, J. C. Collings, D. Albesa-Jové, A. S. Batsanov, J. A. K. Howard, N. J. Taylor, H. M. Kaiser, D. E. Kaufmann, S.-Y. Poon, W.-Y. Wong, C. Jardin, S. Fathallah, A. Boucekkine, J.-F. Halet and T. B. Marder, *Chem.–Eur. J.*, 2006, **12**, 2758–2771.

16 (*a*) M. Lequan, R. M. Lequan and K. C. Ching, *J. Mater. Chem.*, 1991, **1**, 997–999; (*b*) M. Lequan, R. M. Lequan, K. C. Ching, M. Barzoukas, A. Fort, H. Lahoucine, G. Bravic, D. Chasseau and J. Gaultier, *J. Mater. Chem.*, 1992, **2**, 719–725.

17 (*a*) Z.-q. Liu, Q. Fang, D. Wang, G. Xue, W.-t. Yu, Z.-s. Shao and M.-h. Jiang, *Chem. Commun.*, 2002, 2900–2901; (*b*) Z. Liu, Q. Fang, D. Wang, D. Cao, G. Xue, W. Yu and H. Lei, *Chem.–Eur. J.*, 2003, **9**, 5074–5084; (*c*) J. C. Collings, S.-Y. Poon, C. Le Droumaguet, M. Charlot, C. Katan, L.-O. Pålsson, A. Beeby, J. A. Mosely, H. M. Kaiser, D. Kaufmann, W.-Y. Wong, M. Blanchard-Desce and T. B. Marder, *Chem.–Eur. J.*, 2009, **15**, 198–208.

18 (*a*) S. Yamaguchi, S. Akiyama and K. Tamao, *J. Am. Chem. Soc.*, 2001, **123**, 11372–11375; (*b*) S. Yamaguchi, T. Shirasaka, S. Akiyama and K. Tamao, *J. Am. Chem. Soc.*, 2002, **124**, 8816–8817; (*c*) C. R. Wade, A. E. J. Broomsgrove, S. Aldridge and F. P. Gabbaï, *Chem. Rev.*, 2010, **110**, 3958–3984.

19 (*a*) S. Griesbeck, E. Michail, F. Rauch, H. Ogasawara, C. Wang, Y. Sato, R. M. Edkins, Z. Zhang, M. Taki, C. Lambert, S. Yamaguchi and T. B. Marder, *Chem.–Eur. J.*, 2019, **25**, 13164–13175; (*b*) S. Griesbeck, E. Michail, C. Wang, H. Ogasawara, S. Lorenzen, L. Gerstner, T. Zang, J. Nitsch, Y. Sato, R. Bertermann, M. Taki, C. Lambert, S. Yamaguchi and T. B. Marder, *Chem. Sci.*, 2019, **10**, 5405–5422; (*c*) S. Griesbeck, M. Ferger, C. Czernetzi, C. Wang, R. Bertermann, A. Friedrich, M. Haehnel, D. Sieh, M. Taki, S. Yamaguchi and T. B. Marder, *Chem.–Eur. J.*, 2019, **25**, 7679–7688; (*d*) S. Griesbeck, Z. Zhang, M. Gutmann, T. Lühmann, R. M. Edkins, G. Clermont, A. N. Lazar, M. Haehnel, K. Edkins, A. Eichhorn, M. Blanchard-Desce, L. Meinel and T. B. Marder, *Chem.–Eur. J.*, 2016, **22**, 14701–14706; (*e*) J. Liu, X. Guo, R. Hu, X. Liu, S. Wang, S. Li, Y. Li and G. Yang, *Anal. Chem.*, 2016, **88**, 1052–1057.

20 Z. Zhang, R. M. Edkins, J. Nitsch, K. Fucke, A. Eichhorn, A. Steffen, Y. Wang and T. B. Marder, *Chem.–Eur. J.*, 2015, **21**, 177–190.

21 B. Wang, H. Pan, J. Jia, Y.-Q. Ge, W.-Q. Cai, J.-W. Wang and C.-H. Zhao, *Tetrahedron*, 2014, **70**, 5488–5493.

22 P. Gautam, R. Maragani and R. Misra, *RSC Adv.*, 2015, **5**, 18288–18294.

23 S. Yamaguchi and K. Tamao, *Bull. Chem. Soc. Jpn.*, 1996, **69**, 2327–2334.

24 (*a*) T. Baumgartner, *Acc. Chem. Res.*, 2014, **47**, 1613–1622; (*b*) M. Hissler, P. W. Dyer and R. Réau, *Coord. Chem. Rev.*, 2003, **244**, 1–44; (*c*) M. Hissler, C. Lescop and R. Réau, *Pure Appl. Chem.*, 2007, **79**, 201–212; (*d*) T. Baumgartner and R. Réau, *Chem. Rev.*, 2006, **106**, 4691–4727.

25 (*a*) A. Fukazawa, S. Suda, M. Taki, E. Yamaguchi, M. Grzybowski, Y. Sato, T. Higashiyama and S. Yamaguchi, *Chem. Commun.*, 2016, **52**, 1120–1123; (*b*) A. Fukazawa, J. Usuba, R. A. Adler and S. Yamaguchi, *Chem. Commun.*, 2017, **53**, 8565–8568.

26 T. Baumgartner, T. Neumann and B. Wirges, *Angew. Chem., Int. Ed.*, 2004, **43**, 6197–6201.

27 C. Romero-Nieto and T. Baumgartner, *Synlett*, 2013, **24**, 920–937.

28 (*a*) Y. Dienes, S. Durben, T. Kárpáti, T. Neumann, U. Englert, L. Nyulászi and T. Baumgartner, *Chem.–Eur. J.*, 2007, **13**, 7487–7500; (*b*) C. Romero-Nieto, K. Kamada, D. T. Cramb, S. Merino, J. Rodriguez-Lopez and T. Baumgartner, *Eur. J. Org. Chem.*, 2010, 5225–5231.

29 H. V. Huynh, X. He and T. Baumgartner, *Chem. Commun.*, 2013, **49**, 4899–4901.

30 Z. Wu, J. Nitsch, J. Schuster, A. Friedrich, K. Edkins, M. Loebnitz, F. Dinkelbach, V. Stepanenko, F. Würthner, C. M. Marian, L. Ji and T. B. Marder, *Angew. Chem., Int. Ed.*, 2020, **59**, 17137–17144.

31 Y. Niu, W. Li, Q. Peng, H. Geng, Y. Yi, L. Wang, G. Nan, D. Wang and Z. Shuai, *Mol. Phys.*, 2018, **116**, 1078–1090.

32 R. R. Valiev, V. N. Cherepanov, G. V. Baryshnikov and D. Sundholm, *Phys. Chem. Chem. Phys.*, 2018, **20**, 6121–6133.

33 M. J. Frisch, G. W. Trucks, H. B. Schlegel, G. E. Scuseria, M. A. Robb, J. R. Cheeseman, G. Scalmani, V. Barone, G. A. Petersson, H. Nakatsuji, *et al.*, *Gaussian 16, Revision B.01*, Gaussian Inc., Wallingford CT, 2016.

34 X. Gao, S. Bai, D. Fazzi, T. Niehaus, M. Barbatti and W. Thiel, *J. Chem. Theory Comput.*, 2017, **13**, 515–524.

35 (*a*) C. Wang, M. Taki, Y. Sato, A. Fukazawa, T. Higashiyama and S. Yamaguchi, *J. Am. Chem. Soc.*, 2017, **139**, 10374–10381; (*b*) M. Grzybowski, M. Taki, K. Senda, Y. Sato, T. Ariyoshi, Y. Okada, R. Kawakami, T. Imamura and S. Yamaguchi, *Angew. Chem., Int. Ed.*, 2018, **57**, 10137–10141; (*c*) C. Wang, M. Taki, Y. Sato, Y. Tamura, H. Yaginuma, Y. Okada and S. Yamaguchi, *Proc. Natl. Acad. Sci. U. S. A.*, 2019, **116**, 15817–15822.

36 M. Ito, E. Ito, M. Hirai and S. Yamaguchi, *J. Org. Chem.*, 2018, **83**, 8449–8456.

37 M. Hanazawa, R. Sumiya, Y. Horikawa and M. Irie, *J. Chem. Soc., Chem. Commun.*, 1992, 206–207.

38 T. Sumi, Y. Takagi, A. Yagi, M. Morimoto and M. Irie, *Chem. Commun.*, 2014, **50**, 3928–3930.
39 H. Sotome, T. Nagasaka, K. Une, C. Okui, Y. Ishibashi, K. Kamada, S. Kobatake, M. Irie and H. Miyasaka, *J. Phys. Chem. Lett.*, 2017, **8**, 3272–3276.
40 (*a*) Ž. Ban, S. Griesbeck, S. Tomić, J. Nitsch, T. B. Marder and I. Piantanida, *Chem.–Eur. J.*, 2020, **26**, 2195–2203; (*b*) H. Amini, Ž. Ban, M. Ferger, S. Lorenzen, F. Rauch, A. Friedrich, I. Crnolatac, A. Kenđel, S. Miljanić, I. Piantanida and T. B. Marder, *Chem.–Eur. J.*, 2020, **26**, 6017–6028.